Magnetic Resonance in Medicine 51:1163–1172 (2004)

MR-Trackable Intramyocardial Injection Catheter

P.V. Karmarkar,[1*] D.L. Kraitchman,[1] I. Izbudak,[1] L.V. Hofmann,[1] L.C. Amado,[2] D. Fritzges,[1] R. Young,[3] M. Pittenger,[3] J.W.M. Bulte,[1] and E. Atalar[1,4]

There is growing interest in delivering cellular agents to infarcted myocardium to prevent postinfarction left ventricular remodeling. MRI can be effectively used to differentiate infarcted from healthy myocardium. MR-guided delivery of cellular agents/therapeutics is appealing because the therapeutics can be precisely targeted to the desired location within the infarct. In this study, a steerable intramyocardial injection catheter that can be actively tracked under MRI was developed and tested. The components of the catheter were arranged to form a loopless RF antenna receiver coil that enabled active tracking. Feasibility studies were performed in canine and porcine myocardial infarction models. Myocardial delayed-enhancement (MDE) imaging identified the infarcted myocardium, and real-time MRI was used to guide left ventricular catheterization from a carotid artery approach. The distal 35 cm of the catheter was seen under MRI with a bright signal at the distal tip of the catheter. The catheter was steered into position, the distal tip was apposed against the infarct, the needle was advanced, and a bolus of MR contrast agent and tissue marker dye was injected intramyocardially, as confirmed by imaging and postmortem histology. A pilot study involving intramyocardial delivery of magnetically labeled stem cells demonstrated the utility of the active injection catheter system. Magn Reson Med 51: 1163–1172, 2004. © 2004 Wiley-Liss, Inc.

Key words: interventional MRI; intramyocardial injection catheter; labeled stem cells; intramyocardial injections; catheter tracking; cardiac MRI; iron oxide MR contrast agent

Occlusive coronary artery disease (CAD), leading to myocardial infarction and subsequent congestive heart failure, is a major cause of morbidity and mortality in the western world. Because adult cardiomyocytes have a limited ability to regenerate (1), ischemic events often result in irreversible cell injury and concurrent myocardial dysfunction. Much of the treatment of CAD is aimed at restoring blood flow to minimize the loss of functional myocytes. There is growing interest in delivering cellular agents (e.g., mesenchymal stem cells (MSCs), myoblasts, etc.) to the infarcted myocardium to restore healthy myocardial function (2–7). However, delivering such therapeutic agents by an intramyocardial approach requires a suitable imaging modality that can distinguish healthy from infarcted tissue, and guide the procedure.

Interventional cardiology procedures are performed under x-ray fluoroscopic guidance. However, x-ray imaging techniques cannot distinguish between infarcted and healthy myocardium. Cardiac electromechanical mapping systems (e.g., Biosense Webster's NOGA systems (8,9)) have been used to differentiate between healthy and infarcted myocardium. The NOGA system is comprised of a catheter with three coils and an endocardial-potential measuring electrode located at the distal tip. During a typical clinical procedure, three external magnets are placed at different locations around the patient's chest. The catheter is advanced in the left ventricle (LV) and is moved around to record electrical activity, the motion of the distal tip, and the distal-tip location data. A 3D, real-time dynamic reconstruction of the LV, with an assessment of the electrical and mechanical properties of the myocardium, is then created. Healthy, viable tissue is differentiated from infarcted tissue by measuring the endocardial potential and motion at the distal tip of the catheter. Since this system does not provide an anatomical image of the heart, the system requires x-ray guidance to determine the position of the catheter. This procedure is lengthy, and the quality of the map is operator-dependent. On the other hand, MRI offers investigators the ability to readily differentiate healthy from infarcted myocardium with a high degree of anatomical detail using delayed contrast-enhanced imaging (10,11). Moreover, real-time MRI can be used to guide interventional procedures without the use of ionizing radiation. Thus, the clinical efficacy of an intramyocardial delivery therapy may be improved by the use of MRI to guide the delivery to the desired locations in the myocardium.

Currently available injection catheter systems are not suitable for use in an MR environment, for safety and procedural reasons. These catheters are constructed with metallic components, including an injection needle, a pull-wire, and a braided shaft. These components can be ferromagnetic and thus may create a susceptibility artifact and pose a safety hazard in the MR environment. Long metallic wire components in these catheters can couple with the external RF fields, causing localized tissue to heat to unsafe levels (12,13). These catheters, which are also called passive devices, can be visualized on MR images as a signal void or susceptibility artifact, but the weak signal can make determining the precise location of the catheter body and distal tip problematic. The advantage of passive tracking is that no specialized hardware, software, or image postprocessing is needed to "see" these devices.

With active catheter tracking, one can accurately track the position of the catheter without distortion of the underlying anatomy. Active tracking consists of obtaining an MR signal from the catheter located within the native

[1]Department of Radiology, Johns Hopkins University School of Medicine, Baltimore, Maryland.

[2]Cardiology Division, Department of Medicine, Johns Hopkins University School of Medicine, Baltimore, Maryland.

[3]Osiris Therapeutics Inc., Baltimore, Maryland.

[4]Department of Electrical Engineering, Bilkent University, Ankara, Turkey.

Grant sponsor: NIH; Grant numbers: RO1HL61672; RO1HL57483; RO1HL63439.

*Correspondence to: Parag V. Karmarkar, Department of Radiology, Johns Hopkins University, Traylor Building, Room 330, 720 Rutland Ave., Baltimore, MD 21025. E-mail: pkarmar@mri.jhu.edu

Received 9 June 2003; revised 15 January 2004; accepted 16 January 2004.

DOI 10.1002/mrm.20086

Published online in Wiley InterScience (www.interscience.wiley.com).

anatomy. Typically, active tracking requires postprocessing of the images to superimpose the image of the coil on a previously obtained road map image or other hardware modifications. Different types of RF receiver antennas (e.g., loop, loopless, opposed solenoid, etc.) can be incorporated into intravascular catheters to enable active tracking (14–21).

The feasibility of real-time MR-guided intramyocardial injections was demonstrated by Lederman et al. (22), using an MRI-modified commercially available injection catheter (Stiletto™; Boston Scientific, Natick, MA). The Stilleto™ system consists of three separate components: two concentric fixed curve guide catheters (9 Fr and 7 Fr), and an inner spring loaded needle component. The orientation of the guide catheter in the desired direction is achieved by manipulating the positions of the two concentric guide catheters relative to each other, the needle component is then advanced in the guide catheter for intramyocardial delivery of therapeutics (23). Dick et al. (24) reported the use of a MRI-modified Stiletto™ injection catheter system in which the guide catheters are arranged as one RF antenna. The second RF antenna, a microcoil, is built into the distal tip of the injection needle system. This creates a high-intensity signal at the distal tip, to enhance positioning of the needle system before the injection is performed. The limitation of this system is its inability to access the basal anatomy of the left ventricle due to the fixed curve of the LV guide catheters.

In this study, we demonstrate the feasibility of developing a steerable intramyocardial injection catheter with a deflectable distal section, which can be actively tracked and used to deliver cellular therapeutics to the infarcted myocardium under MRI guidance. The components of the catheter are arranged to form a "loopless antenna" RF receiver coil that provides a region of high signal along the length of the coil to enable active tracking. The distal tip of the catheter was modified to create a "coiled tip" that provides high-intensity signal at the distal tip. Thus, the position of the distal tip as it apposes the infarcted myocardium can be visualized before the needle is advanced and the therapeutics are delivered directly into the myocardium. The catheter was tested for mechanical, imaging, and safety performance. As an example of the practical utility of this device, we show here that magnetically labeled MSCs can be delivered and imaged in real time in a canine myocardial infarct model.

THEORY

An intramyocardial injection catheter typically consists of four metallic components: a pull wire, an anchor wire, an injection needle, and a braid over the proximal section of the catheter. The objective of this work was to arrange these components to form an RF receiver antenna, with a high-intensity signal at the distal tip of the catheter coil, while maintaining the desired mechanical properties for intramyocardial LV injections. In this system, the anchor wire is 4 cm long and is located in the distal section of the catheter. It is connected to the distal end of the pull wire and facilitates the deflection of the distal section. The anchor wire has virtually no role to play in the electrical functioning of the catheter, since it is only 4 cm long and is electrically connected to the distal end of the pull wire. Different receiver coil configurations were considered, and a modified loopless antenna design was selected and implemented.

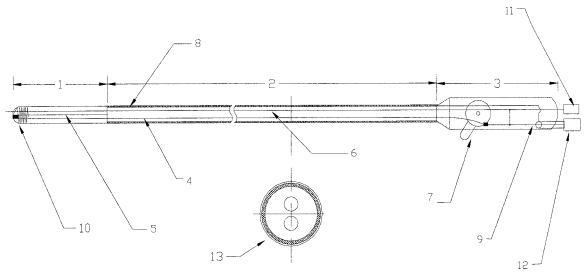

FIG. 1. Schematic of the active injection catheter. The catheter consists of the following components: 1) distal deflectable section, 2) proximal nondeflectable section, 3) handle section, 4) pull wire, 5) anchor wire in the distal section, 6) injection needle, 7) deflection dial, 8) copper braiding (acts as the shielding of the cable), 9) electrical connections, 10) distal coiled tip, 11) hub to connect the syringe to the needle, 12) MMCX connector, and 13) proximal shaft assembly (shown in cross section).

The loopless RF receiver coil dipole antenna, as described by Ocali and Atalar (19) is composed of a coaxial cable with a single metallic core that runs the length of the cable, and further extends a length of $\lambda/4$ beyond the distal end of the cable (shielding). At the proximal end of the coaxial cable, a matching/tuning and decoupling circuit matches the output of the loopless antenna to the desired frequency. For this study, we modified the loopless antenna design by constructing a coaxial cable with two cores (the injection needle and the pull wire) that are insulated from each other (with a 0.7-mm separation between the two cores). The copper braid, in the proximal section of the catheter, forms the shielding of the coaxial cable. Both the cores extend beyond the shielding into the distal deflectable section, where they are electrically insulated by separate polymer tubing housings. One core (the injection needle) is terminated at the distal end of the catheter. The other core (the pull wire) extends beyond the length of the catheter, but is coiled back upon itself to create the "coil tip." The two cores (i.e., the injection needle and the pull wire) are electrically connected at the proximal end of the catheter. A coaxial cable connects the catheter to the matching tuning interface circuit. The core of the coaxial cable is connected to the injection needle and the pull wire, and the shielding of the coaxial cable is connected to the copper braid of the catheter. Thus, our intramyocardial injection catheter coil design can be described as a modified loopless antenna with a coiled tip.

MATERIALS AND METHODS

Catheter Design

A schematic of the steerable injection catheter is shown in Fig. 1. The catheter is ~80 cm long, 0.3 cm (9 French) in diameter, and consists of three sections (a distal deflectable section (4 cm), a fixed proximal section (70 cm), and the handle section). The junction of the distal deflectable section and the proximal nondeflectable section is the

"point of deflection," or fulcrum, at which the distal section of the catheter deflects. The deflection mechanism is comprised of a pull wire, an anchor-wire, and the deflection dial. The pull wire is an 0.035 cm diameter, gold-plated nitinol wire (NDC, Fremont, CA), and the anchor wire is a 0.045 cm diameter nitinol wire. For the deflection mechanism, the anchor wire is 4 cm long and is located in the distal section of the catheter and fixed at two points: one at the fulcrum and the other at the distal tip of the catheter. The pull wire runs along the length of the catheter. The distal end of the pull wire is connected to the distal end of the anchor wire, and the proximal end of the pull wire is connected to the deflection dial to control the extent of deflection. At the distal end of the pull wire, a 10 cm long, 30 American Wire Gauge (AWG) copper magnet wire (Belden, Inc.) is connected and it coils back upon itself over the distal tubing, as shown in Fig. 1. The pull wire, anchor wire, and copper wire from the coiled tip are electrically connected to form a single conductor unit (~95 cm long). The retractable injection needle (26 AWG, nitinol tubing, 90 cm long; NDC, Fremont, CA) runs along the length of the catheter parallel to the pull wire. The distal end of the needle is a three-face bevel to facilitate easy advancement into the myocardium. A hub on the proximal end of the needle serves as a connector to allow connection with the therapeutic medium-filled syringe. The needle can be manually advanced beyond the catheter tip for a distance of 0.5 cm or retracted into the catheter, as desired.

The desired mechanical and electrical properties of the catheter were achieved by placing the metallic components into different polymeric tubings. The proximal shaft consists of dual lumen nylon tubing (0.2 cm diameter): one lumen houses the pull wire, and the other houses the injection needle (MPE Inc., Minneapolis, MN). The dual lumen tubing is covered with a copper braid (32 AWG wire tubular braid; Alpha Wire Company, Elizabeth, NJ). The copper braid is further insulated with a 0.007 cm thick polyimide tubing. In the distal section, the pull wire-anchor wire assembly is housed in thin-walled polytetrafluoroethylene (PTFE) tubing (0.09 cm diameter; Zeus Inc., SC). The needle is housed in a nylon tube (0.08 cm diameter; Zeus Inc., SC). The two tubings run parallel to each other and are housed in flexible nylon tubing (0.3 cm diameter; Putnam Plastics, Inc., NH). The distal and transition sections of the catheter are bonded with adhesive to seal the catheter. The housing of the steering handle is composed of acrylic components. The deflection dial can be rotated to control the extent of deflection of the distal section of the catheter. The nylon stopper and the connector prevent the needle from being extended more than 1 cm beyond the distal tip of the catheter. The needle is advanced manually as required, and is inside the catheter otherwise. The balun decoupling and matching-tuning circuit, as shown in Fig. 2, is implemented to match the output of the catheter coil at 63.86 MHz. The balun circuit acts as an RF trap by preventing the shield currents induced on the coaxial cables, connecting the catheter to the scanner, from reaching the catheter. The decoupling circuit reduces the length of the catheter by $\lambda/4$ at 63.86 MHz during RF transmit, when a DC current is applied to shunt the diode, thus preventing excessive RF deposition and local temperature rise along the length of the catheter.

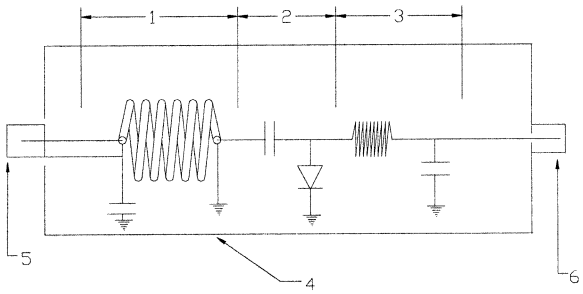

FIG. 2. Schematic of the loopless antenna matching/tuning and decoupling circuit: 1) balun section of the circuit, 2) decoupling section of the circuit, 3) matching/tuning section of the circuit, 4) shielded box, 5) ground isolated micro BNC connector, and 6) BNC connector.

Phantom MRI

All phantom and in vivo imaging was performed on a 1.5 T MR scanner (CV/i; GE Medical Systems, Waukesha, WI). We determined the signal-to-noise ratio (SNR) and heating performance while transmitting with the body coil and receiving with the injection catheter. The SNR properties of the catheter were tested in a saline (0.9%) phantom (45 cm long, 15 cm wide, and 10 cm deep). The catheter was advanced in the phantom for a length of 40 cm and imaged with a fast spin echo (FSE) pulse sequence (TE = 14 ms, TR = 2000 ms, echo train length (ETL) = 16, field of view (FOV) = 24 cm, image matrix = 256 × 256, one excitation number of sequential acquisitions (NSA), and slice thickness (ST) = 5 mm). We tested the signal characteristics of the coil in both straight and deflected states to determine whether the extent of deflection affected the signal profile of the catheter. SNR performance along the length of the catheter was measured on sagittal images acquired with the FSE sequence. SNR was calculated as the ratio of mean signal intensity to the standard deviation (SD) of background signal multiplied by 0.65. We measured the signal intensity profile as a function of distance from the catheter by drawing a line one pixel thick across the sagittal image at the distal tip of the catheter, and at the fulcrum or "junction" of the modified loopless antenna, which was 4 cm proximal to the distal tip of the catheter. The SD of the background signal was measured in a circular region of interest (500 pixels square in area) outside the phantom. The SNR profile plot was obtained as a function of distance from the catheter, as shown in Fig. 3c.

Safety Testing

Heating experiments were performed with the injection catheter in a cylindrical (20 cm diameter, 50 cm long) polyacrylamide gel (VWR International) phantom. The polyacrylamide gel has a conductivity of 0.7 siemens per meter at 63.86 MHz, which simulates the conductivity of human tissue. Fiber-optic temperature measurement probes, with a sensitivity of 0.05°C, were used to measure the local specific absorption rate (SAR). We determined

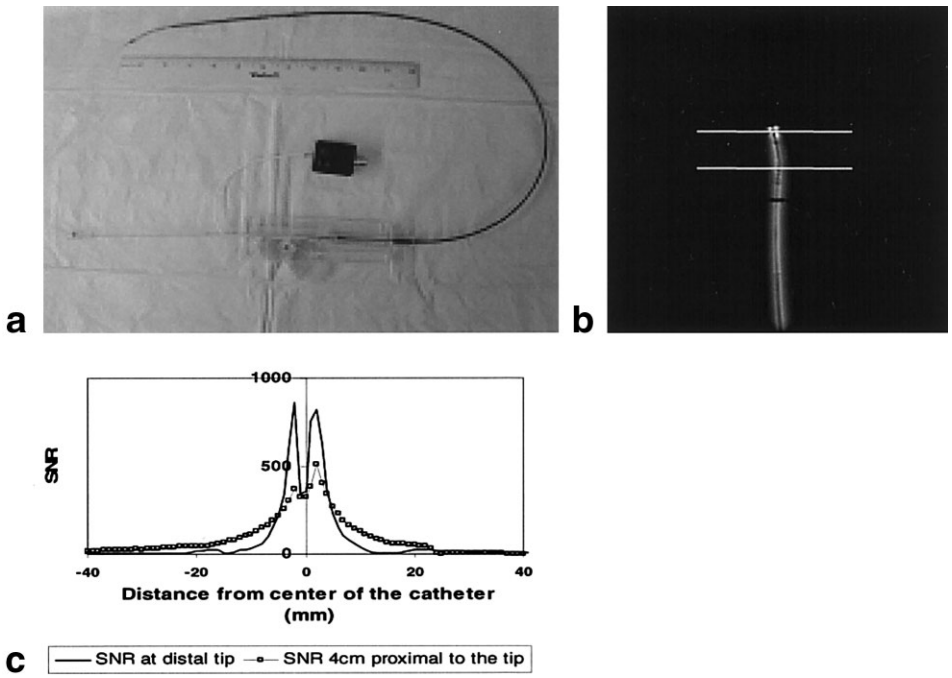

FIG. 3. **a:** Photograph of the injection catheter. **b:** Image acquired by the catheter in a saline phantom, with the entire length of the catheter seen under MR as a bright signal at the distal tip of the catheter. **c:** SNR profile plot along the distal tip and 4 cm proximal to the distal tip. The peak SNR at the distal tip is ~800, and the peak SNR 4 cm proximal to the tip is 500.

the SAR by finding the initial slope of temperature rise (dT/dt) and multiplying by the specific heat of the gel (4180 J/kg). The SAR was monitored with a four-channel fiberoptic thermometer that measured the temperature at each location every 150 ms (UMI4; FISO Technologies, Quebec, Canada). Three probes were positioned along the length of the catheter: at the distal tip of the needle (the needle is advanced 1 cm out of the catheter), at the distal tip of the catheter, and at the fulcrum or point of deflection, which is also the junction of the modified loopless antenna. A fast spoiled gradient echo (FSPGR) pulse sequence (TE = 1.9 ms, TR = 5.8 ms, BW = 128 kHz, FOV = 30 cm, image matrix = 256 × 128, NSA = 113, four axial slices, and ST = 10 mm) resulted in a total imaging time of 10.06 min. The weight of the phantom was set to 250 lb, and the scanning parameters resulted in a peak SAR of 3.98 W/kg, as calculated by the scanner software. The catheter was placed in the polyacrylamide gel phantom, straight, 5 cm from the edge of the phantom, and was advanced 45 cm into the gel. The phantom was placed in the scanner bore such that the catheter was 15 cm off the isocenter. This catheter position was selected to simulate a patient in the scanner with the catheter advanced through the right femoral artery. The following conditions were tested:

1. Needle advanced with the catheter connected to the scanner.
2. Needle retracted into the catheter while connected to the scanner.
3. Catheter disconnected from the scanner with the needle advanced.
4. Needle advanced out of the catheter, and with a thin polyimide insulation/coating on the needle (distal 60 cm).

Animal Experiments

The intramyocardial injection catheter was tested in three closed-chest myocardial infarction animal models (two canine and one porcine). All of the animal protocols were reviewed and approved by our institution's animal care and use committee. Myocardial infarction was created by means of a 90-min, closed-chest balloon occlusion of the left anterior descending (LAD) coronary artery under x-ray fluoroscopy guidance, followed by perfusion. The intramyocardial injections were carried out 2 weeks postinfarction. For MRI, the animals were induced with thiopental (25 mg/kg to effect), intubated, and maintained on isoflurane general anesthesia with mechanical ventilation. A carotid artery cut-down to place a 10 F introducer sheath was performed prior to MRI to facilitate LV catheterization, and the animals were heparinized (5000 IU iv).

Animal MRI

The anesthetized animals were placed in right decubitus with electrocardiogram (ECG) electrodes on their limbs and chest wall for ECG gating. A four-channel, cardiac phased-array coil was placed around the chest. Prior to MR-guided LV catheterization, the location and extent of myocardial infarction was confirmed by myocardial delayed-enhancement (MDE) MRI. Images were acquired 15 min after a 0.2 mmol/kg i.v. bolus of Gd-DTPA (5 cc/s power injection; MedRad, Indianola, PA) was administered. Contiguous short-axis (six to eight slices) and rotating long-axis slices (20–30° rotation angle) were acquired with a breath-hold, ECG-gated, saturation pulse recovery FGRE sequence (TE = 3.3 ms, TR = 7.4 ms, BW = 31.25 kHz, FOV = 28 cm, ST = 8 mm, image matrix = 256 × 190 interpolated to 256 × 256, flip angle = 25°, inversion time (TI) = 200 ms, and two NSA). Breath-

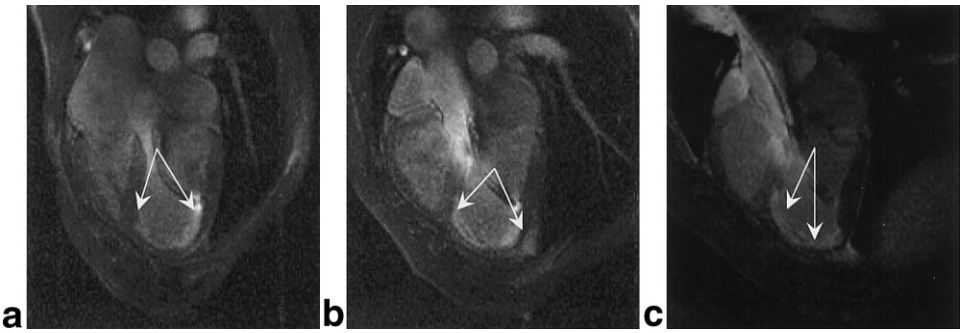

FIG. 4. Parallel long-axis MDE images showing the infarcted sections of the myocardium, as indicated by arrows. **a–c:** The infarction extends from the anterior septum to the lateral wall of the LV. A saturation recovery FGRE sequence (TE = 3.3 ms, TR = 7.4 ms, BW = 31.25 kHz, FOV = 28 cm, ST = 8 mm, image matrix = 256 × 190, flip angle = 25°, TI = 200 ms, and NSA = 2) was used.

holding was achieved by turning off the ventilator during the scan. Images were acquired in mid-diastole. Hyperenhancing tissue was identified as infarcted myocardium, as shown in Fig. 4.

LV Catheterization

Images were acquired with the use of a custom phased-array adapter that combined the signals from the injection catheter and one element each from the anterior and posterior cardiac phased-array coils. The combined image displaying the cardiac anatomy and the catheter was used to guide the procedure. The catheter was advanced into the LV via the carotid introducer, and the distal tip was apposed against the myocardium in the area of interest (infarcted myocardium identified by MDE) with a real-time, steady-state free precession (SSFP) sequence (TR = 3.4 ms, TE = 1.2 ms, flip angle = 45°, BW = 125 kHz, ST = 10 mm, FOV = 28 cm, image matrix = 128 × 128 interpolated to 256 × 256, and NSA = 0.5), which resulted in four frames per second. This sequence was used in conjunction with interactive scan plane acquisition (*i*-Drive; General Electric, Waukesha, WI) to guide the LV catheterization and visualize the test injections. All images were acquired without cardiac gating during free breathing.

Once the distal tip of the catheter was apposed against the myocardium, the needle was advanced into the tissue to a maximal depth of 0.5 cm, and a 0.5-cc volume injection of diluted Gd-DTPA (30 mM dilution with physiologic saline solution) mixed with a tissue marking dye (TMD-5; Triangle Biomedical Sciences, Inc., Durham, NC) was injected into the myocardium. The injection was visualized by means of an SSFP sequence with the flip angle increased to 90°, with and without inversion recovery. In addition, a spoiled gradient echo (SPGR) sequence, with a flip angle of 90°, without inversion recovery was also acquired. Finally, a high-resolution, breath-held, ECG-gated SSFP sequence (TR = 4.5 ms, TE = 1.8 ms, BW = 125 kHz, FOV = 28 cm, image matrix = 256 × 160, ST = 8 mm, and eight views per segment) was acquired with the use of the cardiac coil to confirm the presence of myocardial contrast injections. In one animal, pilot injections of MSCs labeled with an iron oxide contrast agent (Feridex; Berlex Laboratories, Wayne, NJ), were performed following a diluted Gd-DTPA test injection. The MSCs were labeled with the iron contrast marker (Feridex) and poly-L-lysine, by a technique previously described by Frank et al. (25) and implemented by Kraitchman et al. (26) to locate the labeled MSCs in the myocardium by MRI.

Postmortem Techniques

After the animals were humanely euthanized, the hearts were excised, fixed in formalin, and sectioned either along the short-axis image planes or a single long-axis imaging plane, corresponding to the injection locations. The tissue-dye location was confirmed and compared with the MRI injection sites. Postmortem heart slices were captured with a digital camera.

RESULTS

A photograph of the intramyocardial injection catheter with the modified loopless antenna receiver coil is shown in Fig. 3a. The impedance of the modified coaxial cable was 40 ohms when the needle and the pull wire were connected at the proximal end. The impedance of the coaxial assembly with individual pull wire and the needle was 40 ohms and 37 ohms, respectively.

Phantom Studies

An image acquired by the injection catheter, with the needle advanced 0.5 cm, is shown in Fig. 3b. The distal 35 cm of the catheter could be seen under MR. In the loopless antenna design, the shield of the coaxial cable acts as a component of the antenna, and consequently the MR signal can be seen for 30 cm on the shielding of the coaxial cable. The signal from the catheter remained consistent whether the catheter was straight or deflected. The SNR profile plot, which is a function of signal drop-off from the catheter, is shown in Fig. 3c. The peak SNR, as measured from the SNR profile plot, was 60% higher at the distal coiled tip compared to the SNR at 4 cm proximal to the distal tip.

Heating Tests

The SAR results are summarized in Table 1. The maximum local SAR was observed when the catheter was not connected to the scanner, with the needle advanced 1 cm out of the catheter and no insulation on the needle. This SAR was 209 W/kg at the distal tip of the catheter, and 105 W/kg at the distal tip of the needle. Under the same conditions, when the catheter was connected to the scanner, the maximum SAR observed was 17 W/kg and

Table 1
Local SAR as Measured for Different Conditions

Condition tested	SAR at distal tip of needle	SAR distal tip of catheter	SAR at the fulcrum (junction of loopless antenna)
No insulation on needle and needle advanced 1 cm	17 W/kg	8.3 W/kg	8.9 W/kg
No insulation on needle and needle retracted in the catheter	N/A	8.3 W/kg	8.9 W/kg
No insulation on needle, needle advanced 1 cm and disconnected from the scanner	105 W/kg	209 W/kg	12.5 W/kg
Needle insulated and needle advanced 1 cm	1.4 W/kg	2.4 W/kg	5.5 W/kg
Needle insulated and retracted in the catheter	N/A	2.4 W/kg	5.6 W/kg

8.3 W/kg at the distal tip of the needle and catheter, respectively. However, with a thin insulation on the needle, the SAR was 1.4 W/kg and 2.4 W/kg at the distal tip of the needle and catheter, respectively. The local SAR at the junction of the catheter (loopless antenna) was 9 W/kg with no insulation on the needle, and 5.5 W/kg with the needle insulated.

Catheter Visualization

The infarcted myocardium was first identified as hyperenhancing tissue, by MDE imaging, as shown in Fig. 4. The LV catheterization was performed with the use of a long-axis imaging plane that showed the infarcted myocardial sections and portions of the aortic root, ascending aorta, and descending aorta (Fig. 5a). The distal 15–25 cm of the catheter could be seen under MR as a bright signal at the "coiled tip" of the catheter. The catheter could be seen in dynamic situations (e.g., when the catheter was deflected to pass the aortic valve or steered into the long-axis imaging plane). Representative images demonstrating LV catheterization with MR guidance and positioning of the distal tip against the infarcted myocardium are shown in Fig. 5. The catheter and the distal tip could be seen as the catheter was advanced through the aortic arch, avoiding the descending aorta and into the ascending aorta, and traversing the aortic valve into the LV (Fig. 5b–d). Once in the LV, the catheter was manipulated so that the distal section of the catheter was in the long-axis imaging plane (Fig. 5e). The catheter was positioned such that the distal tip was apposed against the infarcted myocardium in the septal wall (Fig. 5f). Different long-axis views could be selected, and the catheter could be steered into these planes to access other myocardial segments (Fig. 6a). The location of the distal tip against the myocardium was confirmed by long- and short-axis views.

Injection Visualization

After LV catheterization, injections were performed with the distal tip of the catheter apposed against the infarcted

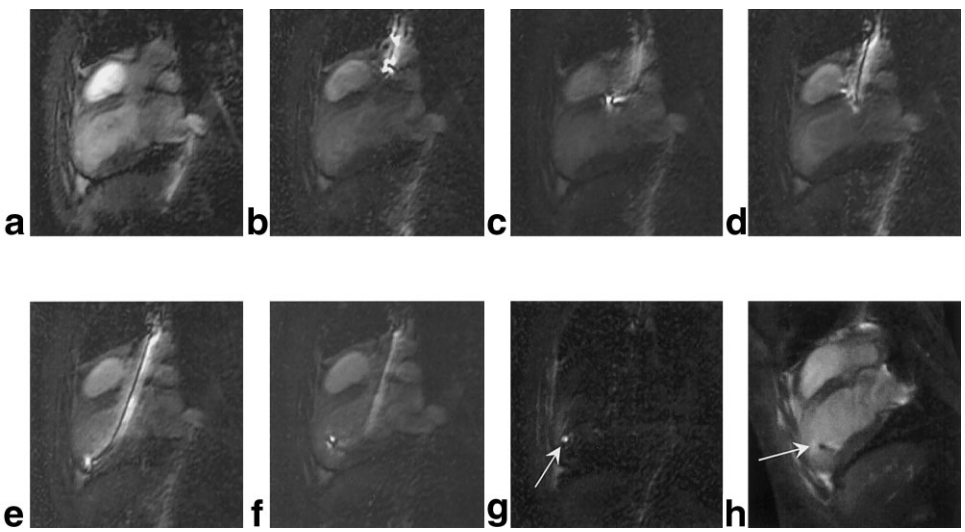

FIG. 5. Still frames depict the catheter being steered toward the infarct in the apical septum under real-time MR guidance, a 30-mM Gd-DTPA injection being administered, and the presence of the injection confirmed by gated, breath-held SSFP imaging. Shown are (**a**) the infarcted septal wall as seen under real-time MRI, (**b**) the catheter being steered in the ascending aorta toward the LV, (**c**) the distal tip at the aortic valve, (**d**) the aortic valve being traversed, (**e**) the distal tip of the catheter at the apex, (**f**) a deflectable catheter with the tip flexed against the infarcted myocardium, (**g**) a 0.5-cc injection of Gd-DTPA (with tissue marker dye) visualized by increasing the flip angle to 90° and switching inversion recovery on, and (**h**) the presence of the injection confirmed by gated, breath-held SSFP imaging (TR = 4.5 ms, TE = 1.8 ms, BW = 125 kHz, FOV = 28 cm, image matrix = 256 × 160, ST = 8 mm, and eight views per segment). The imaging sequence to guide the procedure was as follows: nongated, free-breathing, real-time SSFP with TR = 3.4 ms, TE = 1.2 ms, flip angle = 45°, BW = 125 kHz, ST = 10 mm, FOV = 28 × 21 cm, image matrix = 128 × 128, and NSA = 0.5.

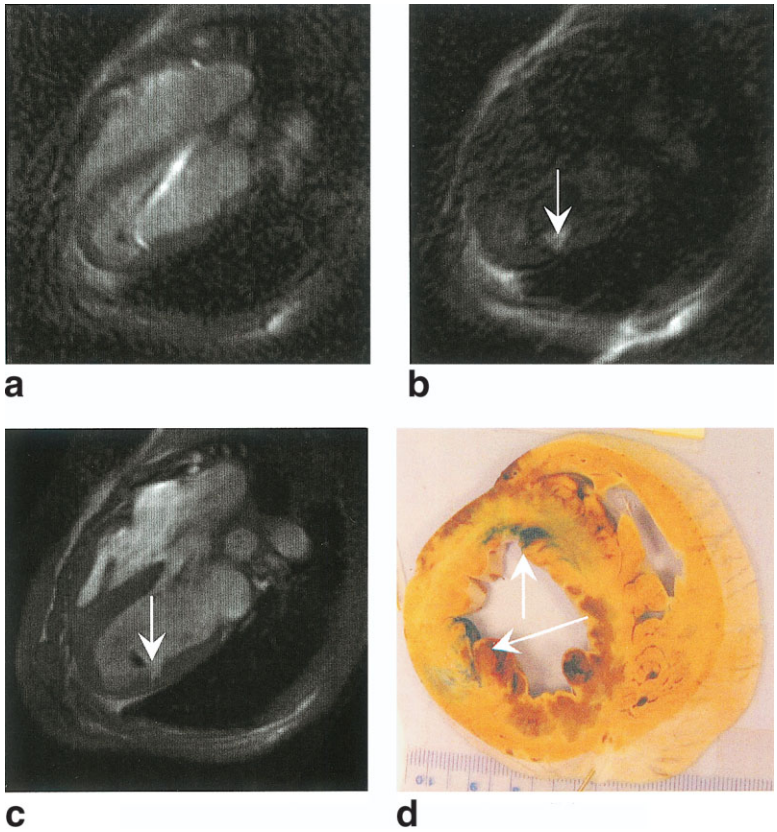

FIG. 6. Contrast delivery in the lateral wall. **a:** The catheter was torqued toward the infarct in the lateral wall. **b:** An injection of 30 mM Gd-DTPA under real-time MR guidance was carried out as indicated by the arrow. **c:** The injection was confirmed by gated, breath-held SSFP imaging, as indicated by the arrow. **d:** The location of the injections was confirmed by postmortem histology, and both of the injections (i.e., the septal wall and the lateral wall injections) are seen in postmortem sections. The imaging sequences are identical to those used in Fig. 5.

myocardium. The distal tip location was confirmed in short- or long-axis views by high-resolution, ECG-gated, breath-held, SSFP imaging (Fig. 7a). The needle was then advanced into the myocardium to a depth of 0.5 cm, and 1.0 cc of diluted Gd-DTPA, mixed with a tissue marker dye, was injected. We were able to appreciate the enhanced visualization of the injection using a high flip angle combined with an SPGR pulse sequence (Figs. 5g

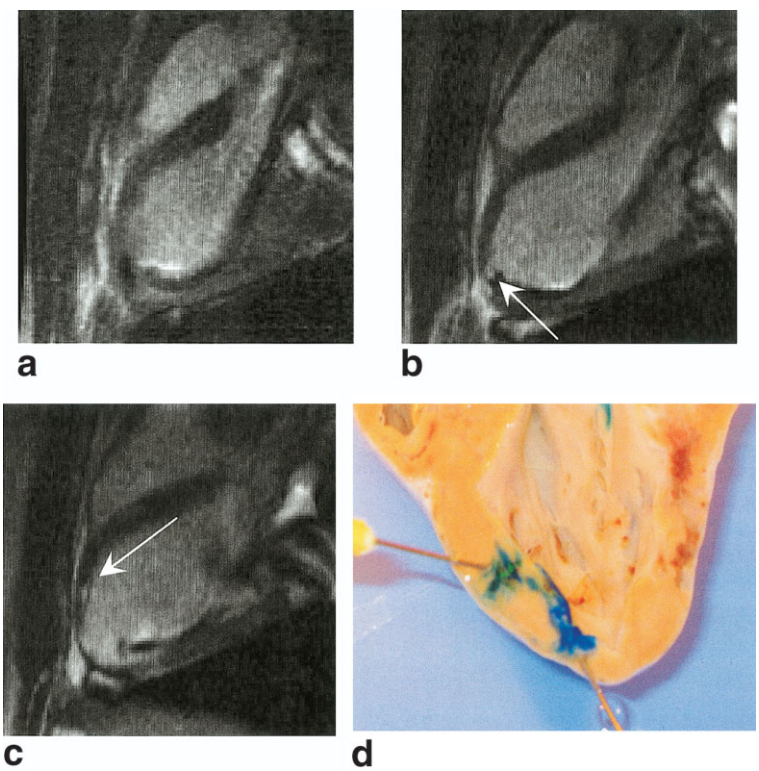

FIG. 7. Gated, breath-held SSFP images of contrast + tissue marker dye injections in the apical septal wall in a porcine model. **a:** Long-axis view image before contrast injections. **b:** The same long-axis views following the first (contrast + blue dye) injection, where the contrast is seen as a hyperintense signal indicated by an arrow. **c:** Long-axis image visualizing the second (contrast + green dye) injection (indicated by an arrow), with the previous contrast injection seen at the apex. **d:** Both injections are confirmed by histology. Imaging sequences are identical to those used in Fig. 5h.

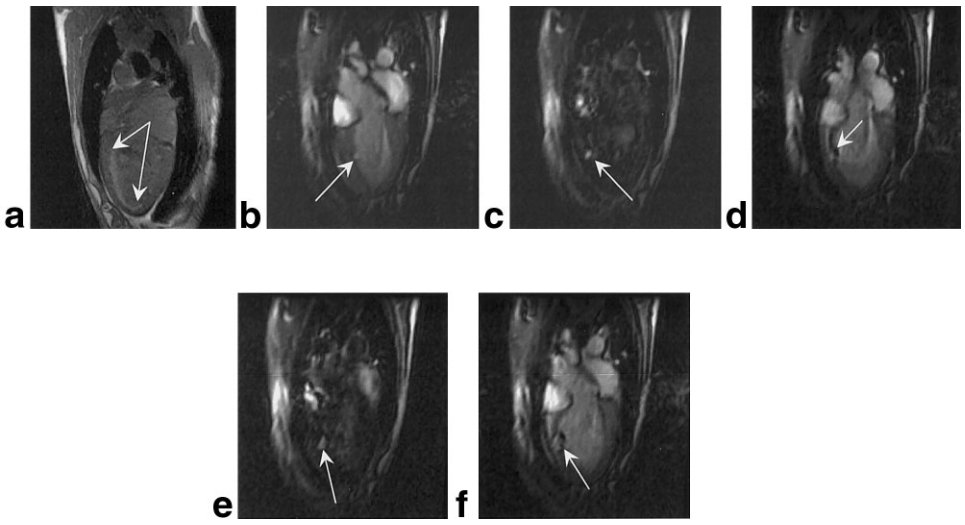

FIG. 8. Representative injections of Feridex-labeled MSCs into the myocardium. **a:** Still frames depicting the infarcted myocardium highlighted by MDE imaging and indicated by arrows. **b:** The distal tip of the catheter is apposed against the infarct in the mid-apical septum under real-time MR guidance. **c:** A 30-mM Gd-DTPA injection is carried out and visualized as a hyperintense lesion. **d:** Feridex-labeled MSCs (7×10^6) are injected at the same location. **e:** The catheter was then repositioned below the previous injection site, and 30 mM Gd-DTPA were injected. **f:** Feridex-labeled MSCs (3×10^6 labeled, and 4×10^6 unlabeled) are injected at the same location, and both injections are visualized (the Gd-DTPA injection is bright, and the hypointense Feridex-labeled MSC injection is dark). The lower concentration of labeled MSCs can be appreciated as a less hypointense lesion in the more apical injection. All of the images were acquired with the use of a real-time SSFP sequence (TR = 3.4 ms, TE = 1.2 ms, FA = 45° (90° for **c** and **e**), BW = 125, image matrix = 128×128, NEX = 0.5) and the *i*-Drive interface to guide the procedure.

and 6b). Postcontrast, SSFP-gated, breath-held, short- and long-axis images confirmed the presence of the contrast agent at the injection site, as seen in low-resolution, nongated, free-breathing images acquired in real time (Figs. 5h and 6c). All of the injections were confirmed by postmortem histology, as shown in Figs. 6d and 7d. All 12 diluted Gd-DTPA injections delivered in two animals were confirmed postmortem. However, only nine injections were visualized during real-time acquisition and high-resolution SSFP imaging. The tissue marker dye diffused in a radial fashion from the injection site. In addition, injections in the septal and lateral walls postmortem are shown in Figs. 6d and 7d.

To demonstrate a practical application for the catheter, we injected Feridex-labeled MSCs in vivo into infarcted canine myocardium. LV catheterization was performed in a manner identical to that in which the animals received noncellular injections. The distal tip of the catheter was positioned within the infarct site, the needle was advanced, and a test injection of 0.5 cc of diluted Gd-DTPA was performed and visualized with a 90° flip angle SPGR sequence. Subsequently, we performed a 0.5-cc injection of Feridex-labeled MSCs (14×10^6 MSC s/ml) without withdrawing the needle. The needle was retracted and the catheter was advanced in the same plane toward the apex, and another 0.5 cc injection (containing approximately 4×10^6 Feridex-labeled MSCs and 3×10^6 unlabeled MSCs in a 0.5-cc volume) was performed. The contrast injection was visualized as hyperintense foci with high-flip-angle SPGR imaging. With the SSFP real-time imaging sequence, the labeled stem cells were seen as a hypointense region (Fig. 8d and e).

DISCUSSION

We developed an active intramyocardial injection catheter with a deflectable distal section, by arranging/configuring the components of the catheter to form a modified loopless antenna. We further demonstrated that the catheter is capable of accurately delivering cellular therapeutics to the infarcted myocardium. Moreover, this design is flexible, and one can incorporate additional needles or deflection mechanisms without changing the basic design. The SNR at the distal tip of the catheter was higher (by ~60%) than at the rest of the catheter. Moreover, the signal from the distal 35-cm length of the catheter facilitated proper positioning, and the bright tip allowed accurate anatomic placement. Our method of active tracking has the advantage of utilizing high signal from the catheter to visualize the catheter within the surrounding tissue/anatomy without the use of specialized hardware or software modifications. Although passive catheter devices can be seen on the image itself, the signature of these passive markers is often insufficient for accurate localization of the catheter tip, which is important for a therapeutic injection application (as demonstrated in this study). Like passive catheter devices, our active catheter approach has the advantage that images of the anatomy and the catheter can be reconstructed using standard software, with the additional benefit of precise tip localization.

Devices containing long metallic components have the potential to heat up in an MR environment. The heating potential depends upon the length of the components and the insulation/dielectric thickness surrounding the components. Since the long metallic wire components of the injection catheter are arranged to form a modified loopless

receiver antenna, and are decoupled when they are connected to the scanner during RF transmit, the localized heating observed along the length of the catheter is significantly lower when the catheter is connected (decoupled) than when it is disconnected from the scanner (not decoupled). When the catheter was not decoupled, the maximum SAR (209 W/kg) was observed at the distal tip of the catheter. This is because the catheter behaves like a linear conductor in the RF field, and since the pull wire with the coiled tip is the longest conductor, maximum SAR is observed at the distal tip of the catheter. With the catheter decoupled during RF transmit, the maximum local SAR (17 W/kg) was observed at the distal tip of the needle, indicating the effectiveness of the decoupling circuit. However, when a needle with a thin insulation was used, the SAR at the tip of the needle was 1.4 W/kg. This also suggests that the heating potential can be further reduced by increasing the insulation thickness over the needle and the proximal section of the catheter. This change may further reduce the SNR along the length of the catheter, making the distal tip appear brighter. However, this would increase the catheter diameter, which would be a limitation for percutaneous vascular procedures.

The mechanical and imaging performance of the catheter was satisfactory. The catheter could be easily seen on MRI and advanced into the LV after it traversed the aortic valve, and accurately positioned for injection at various locations in the LV. The mechanical properties of the catheter make it steerable (deflectable and torquable), so most of the LV can be accessed. All of the injections of diluted Gd-DTPA with tissue dye were confirmed postmortem. However, 25% of the injections were not visualized with the high-temporal-resolution, low-spatial-resolution, real-time SSFP pulse sequence. Because the long-axis planes were chosen to optimize conventional anatomical views (e.g., two- or four-chamber views), in some cases the imaging planes were not optimized for injection visualization. Injection visualization may be improved by the use of a nonconventional imaging plane, a thicker imaging slice, or multislice imaging. Evaluation of postmortem slices revealed that the spreading of the injection was nonuniform from the base to the apex and circumferentially, possibly due to the variation of muscle sheet planes and fibers within the myocardium. Thus, unless expectations of the spread of the injection are taken into account, it is possible that the injection may not be visualized due to partial volume effects.

Although the catheter was designed to deliver therapeutics to the myocardium, additional modifications to our prototype can be incorporated to make the procedure more efficient and precise. In the current design, the distal tip of the needle is not visible on MRI; a coiled tip on the needle could be implemented to increase the signal from the needle and make it visible. A potential advantage of using an active needle is that it eliminates the need for an MR contrast injection to confirm the intramyocardial needle tip location, and thus also eliminates the need for contrast injection. The catheter could also be modified to measure an endocardial potential (EP), to verify contact with the myocardium, and, perhaps, myocardial viability. An RF splitting circuit, similar to that reported by Susil et al. (27), could be implemented to measure the local EP signal at the distal tip of the catheter and confirm the location of the needle within the myocardium.

CONCLUSIONS

We have successfully designed and developed an intramyocardial injection catheter that can be tracked under MRI to deliver therapeutics to the myocardium. The catheter was tested for its ability to deliver labeled stem cells into the targeted regions of the infarcted myocardium.

ACKNOWLEDGMENTS

The authors thank Michelle Marcelino, Christopher Yeung, Tom Foo, and Pelin Aksit for assistance with the experiments, and Mary McAllister for editorial assistance.

REFERENCES

1. Soonpaa MH, Kim KK, Pajak L, Franklin M, Field LJ. Cardiomyocyte DNA synthesis and binucleation during murine development. Am J Physiol 1996;271:H2183–H2189.
2. Taylor DA. Cellular cardiomyoplasty with autologous skeletal myoblasts for ischemic heart disease and heart failure. Curr Control Trials Cardiovasc Med 2001;2:208–210.
3. Orlic D, Kajstura J, Chimenti S, Jakoniuk I, Anderson SM, Li B, Pickel J, McKay R, Nadal-Ginard B, Bodine DM, Leri A, Anversa P. Bone marrow cells regenerate infarcted myocardium. Nature 2001;410:701–705.
4. Toma C, Pittenger MF, Cahill KS, Byrne BJ, Kessler PD. Human mesenchymal stem cells differentiate to a cardiomyocyte phenotype in the adult murine heart. Circulation 2002;105:93–98.
5. Orlic D, Hill JM, Arai AE. Stem cells for myocardial regeneration. Circ Res 2002;91:1092–1102.
6. Al Radi OO, Rao V, Li R-K, Yau T, Weisel RD. Cardiac cell transplantation: closer to bedside. Ann Thorac Surg 2003;75:S674–677.
7. Shake JG, Gruber PJ, Baumgartner WA, Senechal G, Meyers J, Redmond JM, Pittenger MF, Martin BJ. Mesenchymal stem cell implantation in a swine myocardial infarct model: engraftment and functional effects. Ann Thorac Surg 2002;73:1919–1926.
8. Ben-Haim SA, Osadchy D, Schuster I, Gepstein L, Hayam G, Josephson ME. Nonfluroscopic, in vivo navigation and mapping technology. Nat Med 1996;2:1393–1395.
9. Kornowski R, Leon MB, Fuchs S, Vodovotz Y, Flynn MA, Gordon DA, Pierre A, Kovesdi I, Keiser JA, Epstein SE. Electromagnetic guidance for catheter based transendocardial injection: a platform for intramyocardial angiogenesis therapy. Results in normal and ischemic porcine models. J Am Coll Cardiol 2000;35:1031–1039.
10. Kim RJ, Hillenbrand HB, Judd RM. Evaluation of myocardial viability by MRI. Herz 2000;25:417–430.
11. Kim RJ, Wu E, Rafael A, Chen EL, Parker MA, Simonetti O, Klocke FJ, Bonow RO, Judd RM. The use of contrast-enhanced myocardial imaging to identify reversible myocardial dysfunction. N Engl J Med 2000; 243:1445–1453.
12. Nitz WR, Oppelt A, Renz W, Manke C, Lenhart M, Link J. On the heating of linear conductive structures as guide wires and catheters in interventional MRI. J Magn Reson Imaging 2001;13:105–114.
13. Liu CY, Farahani K, Lu DS, Duckwiler G, Oppelt A. Safety of MRI-guided endovascular guidewire applications. J Magn Reson Imaging 2000;12:75–78.
14. Atalar E, Bottomley PA, Ocali O, Correia LC, Kelemen MD, Lima JA, Zerhouni EA. High resolution intravascular MRI and MRS by using a catheter receiver coil. Magn Reson Med 1996;:36:596–605.
15. Martin AJ, Henkelman RM. Intravascular MR imaging in a porcine animal model. Magn Reson Med 1994;32:224–229.
16. Hurst GC, Hua J, Duerk JL, Cohen AM. Intravascular (catheter) NMR receiver probe: preliminary design analysis and application to canine iliofemoral imaging. Magn Reson Med 1992;24:343–357.

17. Zhang Q, Wendt M, Aschoff AJ, Lewin JS, Duerk JL. A multielement RF coil for MRI guidance of interventional devices. J Magn Reson Imaging 2001;14:56–62.
18. Ladd ME, Zimmermann GG, Quick HH, Debatin JF, Boesiger P, von Schulthess GK, McKinnon GC. Active MR visualization of a vascular guidewire in vivo. J Magn Reson Imaging 1998;8:220–225.
19. Ocali O, Atalar E. Intravascular magnetic resonance imaging using a loopless catheter antenna. Magn Reson Med 1997;37:112–118.
20. Dumoulin CL, Souza SP, Darrow RD. Real-time position monitoring of invasive devices using magnetic resonance. Magn Reson Med 1993;29:411–415.
21. Ackerman JL, Offutt MC, Buxton RB, Brady TJ. Rapid 3D tracking of small RF coils [abstract]. In: Proceedings of the 5th Annual Meeting of SMRM, Montreal, Canada, 1986. p 1131.
22. Lederman RJ, Guttman MA, Peters DC, Thompson RB, Sorger JM, Dick AJ, Raman VK, McVeigh ER. Catheter-based endomyocardial injection with real-time magnetic resonance imaging. Circulation 2002;105: 1282–1284.
23. Sherman W. Cellular Therapy for Chronic Myocardial Disease: Nonsurgical Approaches. Basic Appl Myol 2003;13:11–14.
24. Dick AJ, Guttman MA, Raman VK, Peters DC, Pessanha BSS, Hill JM, Smith S, Scott G, McVeigh ER, Lederman RJ. Magnetic resonance fluoroscopy allows targeted delivery of mesenchymal stem cells to infarct borders in swine. Circulation 2003;108:2899–2904.
25. Frank JA, Miller BA, Arbab AS, Zywicke HA, Jordan EK, Lewis BK, Bryant Jr LH, Bulte JWM. Clinically applicable labeling of mammalian cells by combining superparamagnetic iron oxides and transfection agents. Radiology 2003;228:480–487.
26. Kraitchman DL, Heldman AW, Atalar E, Amado LC, Martin BJ, Pittenger MF, Hare JM, Bulte JWM. In vivo magnetic resonance imaging of mesenchymal stem cells in myocardial infarction. Circulation 2003; 107:2290–2293.
27. Susil RC, Yeung CJ, Halperin HR, Lardo AC, Atalar E. Multifunctional interventional devices for MRI: a combined electrophysiology/MRI catheter. Magn Reson Med 2002;47:594–600.